

1      **Simulating the transportation and dispersal of volcanic**  
2      **ash cloud with initial condition created by 3D plume**  
3      **model**

4      **Key Points:**

- 5      • Creating initial conditions for volcanic ash transport and dispersal models based  
6      on 3D plume model output eliminates the need for assumptions or inversion re-  
7      garding initial ash particle distribution with height, and improves prediction ca-  
8      pability.  
9      • Initial particle distribution in vertical direction has greater impact on transport  
10     of ash clouds than does horizontal distribution.  
11     • Ash particles involved in long-range transport are initially concentrated in the um-  
12     brella cloud of large eruptions.

13 **Abstract**

14 VATDs (volcanic ash transportation and dispersion) model atmospheric transport of ash  
 15 starting from a source originating at the volcano represented by concentrations of ash  
 16 with height. Most VATD models use a source of some prescribed shape calibrated against  
 17 an empirical expression for the height-mass eruption rate (MER) relation. The actual  
 18 vertical ash distributions in volcanic plume usually vary from case to case and have com-  
 19 plex dependencies on eruption source parameters and atmospheric conditions. We present  
 20 here for the first time the use of 3D (three-dimensional) plume models to represent ash  
 21 cloud sources without any assumption regarding plume geometry. By eliminating assumed  
 22 behavior associated with the semiempirical plume geometry, the predictive skill of VATD  
 23 simulations are greatly improved. To date no VATD simulation adopts the initial con-  
 24 dition created from first principles based 3D plume simulation. We use our recently de-  
 25 veloped volcanic plume model based on a 3D Lagrangian method [Cao et al, Geophys-  
 26 ical Model Dev., 2018] and couple the output to a standard Lagrangian VATD model  
 27 and apply to historical eruptions to illustrate the effectiveness of this approach. The im-  
 28 portance of the source model is shown in sensitivity analyses which prove that volcanic  
 29 ash transportation simulation is much more sensitive to the source geometry than all other  
 30 input parameters. Further investigation also reveals that initial particle distribution in  
 31 vertical direction has more impact on transportation of ash clouds than horizontal dis-  
 32 tribution. Comparison also indicates that ash particles are concentrated along the in-  
 33 trusion height of umbrella cloud that is much lower than the plume top, which is just  
 34 momentum overshoot.

35 **1 Introduction**

36 **1.1 Volcanic Ash Transportation Forecast**

37 The fine-grain fraction of tephra (volcanic ash) can be widely dispersed, and can  
 38 lead to a degradation of air quality and pose threats to aviation (Tupper et al., 2007).  
 39 Identification of volcanic ash helps schedule flights to avoid areas where ash is present.  
 40 Numerical estimation of ash distribution using known and forecast wind fields is nec-  
 41 essary if we are to accurately predict ash cloud evolution. Numerous VATD (volcanic ash  
 42 transportation and dispersion) models have been developed by both civil and military  
 43 aviation or meteorological agencies to provide forecasts of ash cloud motion (Witham  
 44 et al., 2007). New techniques have been integrated with VATDs to satisfy increasing de-  
 45 mands for more outputs, model accuracy and forecast reliability. This contribution ex-  
 46 plores a method for creating initial conditions for VATD simulations, which promises to  
 47 improve prediction capability and accuracy.

48 ? and Stohl et al. (2011) showed that initial source conditions have significant ef-  
 49 ffects on simulation of volcanic ash transportation. Traditional VATD simulation requires  
 50 key global descriptors of the volcanic plumes, especially plume height, grain size, erup-  
 51 tion duration and mass loading, or alternatively, a mass eruption rate (MER). No mat-  
 52 ter how these global descriptors are obtained, they are used to furnish the initial con-  
 53 ditions for VATDs in the form of a line-source term of a spatio-temporal distribution of  
 54 particle mass. It is a common practice to pick values for these global descriptors using  
 55 an empirical expression for the height-MER relation. The empirical expression is writ-  
 56 ten as a function of several parameters, including the key global descriptors. The val-  
 57 ues for the descriptors can also be found by parameter calibration (e.g. ??Stohl et al.,  
 58 2011; Zidikheri et al., 2017). 1D plume models serve as an alternative option to provide  
 59 values. For example, ? and “stefanescu2014temporal” (n.d.) used the 1D model puffin  
 60 (Bursik, 2001) to generate estimates of mass eruption rate and grain size. In some cases,  
 61 an extra step is adopted to spread ash particles from the line source horizontally, result-  
 62 ing in an initial ash cloud in 3D space. The horizontal spreading depends on an empir-  
 63 ical expression. For example, the VATD model Puff spreads particles from the line source

uniformly in the horizontal direction within a given radius using an empirical expression in puffin. Considering the complexities of volcanic eruptions, the actual ash distribution in initial ash clouds should vary from case to case and with time, making it difficult to find one general expression that is suitable for all cases. It is useful therefore to investigate alternative ways for creating initial ash clouds without assumptions regarding plume geometry or numerical inversion. This provides the major motivation of this paper.

## 1.2 Numerical Tools

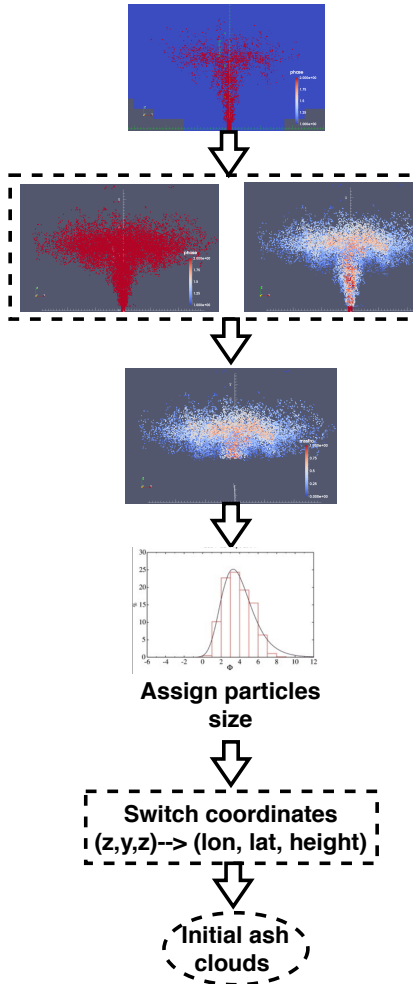
VATD models can be categorized into Lagrangian particle tracking and Eulerian advection-diffusion types. Among several available particle tracking models (e.g. Walko et al., 1995; Searcy et al., 1998; D'amours, 1998; Draxler & Hess, 1998) and advection-diffusion models (e.g. Bonadonna & Houghton, 2005; Folch et al., 2009; Schwaiger et al., 2012), we adopt a particle tracking model, Puff (Tanaka, 1991; Searcy et al., 1998), as the VATD model. Puff can take 3D ash clouds as initial conditions, which makes it technically easier to couple with 3D plume models. Puff initializes a discrete number of tracers that represent a sample of the eruption cloud, and calculates transport, turbulent dispersion, and fallout for each representative tracer. A cylinder emanating vertically from the volcano summit to a specified maximum height is the standard approach to provide a simple model of the geometry of a typical ash column. Puff minimally requires horizontal wind field data. The “restart feature” of Puff makes it technically feasible to accommodate the hand-off between a plume simulation and the Puff simulation in terms of time and length scales.

Besides parameter calibration, 1D (one dimensional) plume models have been used to obtain global descriptors of volcanic plumes. 1D plume models (e.g. Woods, 1988; Bur-sik, 2001; Mastin, 2007; de'Michieli Vitturi et al., 2015; Folch et al., 2016; Pouget et al., 2016) solve the equations of motion in 1D using simplifying assumptions, and hence depend on estimation of certain parameters, especially those related to the entrainment of air, which is evaluated based on two coefficients: a coefficient due to turbulence in the rising buoyant jet, and one due to the crosswind field. Different 1D models adopt different entrainment coefficients based on a specific formulation or calibration against well-documented case studies. The feedback from plume to atmosphere is usually ignored in 1D models. While these 1D models generated well-matched results with 3D models for plumes that are dominated by wind (often called weak plumes) much greater variability is observed for strong plume scenarios (Costa et al., 2016). On the other hand, 3D numerical models for volcanic plumes based on first principles and having few parametrized coefficients (Oberhuber et al., 1998; Neri et al., 2003; Y. J. Suzuki et al., 2005; Cermi-nara, Esposti Ongaro, & Berselli, 2016; Cao et al., 2018) naturally create a 3D ash cloud, which could serve directly as an initial state of the volcanic material for VATDs. How-ever, there is no VATD simulation using such 3D ash clouds as initial conditions. In this paper, we will carry out VATD simulations using an initial state for the ash cloud based on 3D plume simulations, generated with Plume-SPH (Cao et al., 2018; ?). The imple-mentation techniques described in this paper can be applied for any combination of VATD model and 3D plume model even though our investigation is based on a specific VATD model and plume model.

Another popular VATD model hysplit (??) is also used in this study to better un-derstand simulation results by Puff.

## 1.3 Pinatubo Eruption

The 1991 eruption of Pinatubo volcano is used as a case study. Pinatubo erupted between June 12 and 16, 1991, after weeks of precursory activity. The climactic phase started on June 15 at 0441 UTC and ended around 1341 UTC (?). The climactic phase generated voluminous pyroclastic flows, and sent Plinian and co-ignimbrite ash and gas



123      **Figure 1.** Workflow to create initial condition for Puff based on raw output of Plume-SPH  
 124      (Cao et al., 2018). Top: raw output of Plume-SPH. Blue particles are phase 1 (ambient air), red  
 125      particles are phase 2 (erupted material). Second row: plume after removing SPH particles of  
 126      phase 1. Left: colored according to mass fraction of erupted material. Third row: volcanic plume  
 127      above the “corner” region after cutting off the lower portion.

114      columns to great altitudes (?). The evolution of the Pinatubo ash and  $SO_2$  clouds was  
 115      tracked using visible (?), ultraviolet (Total Ozone Mapping Spectrometer; TOMS) (?)  
 116      and infrared sensors, including the Advanced Very High-Resolution Radiometer (AVHRR)  
 117      (?). There is also sufficient observational data to estimate the eruption conditions for  
 118      the climactic phase of the eruption (Y. Suzuki & Koyaguchi, 2009). The availability of  
 119      calibrated eruption conditions and extensive observational data regarding ash clouds trans-  
 120      port make the Pinatubo eruption an ideal case study.

## 121      2 Setting up Simulations

### 122      2.1 Creation of Initial Ash Cloud

128      The steps to create an initial ash cloud based on the raw output of Plume-SPH are  
 129      shown in Fig. 1. The method proposed consists in generating the initial ash cloud di-  
 130      rectly from Plume-SPH, foregoing assumptions and estimates or inverse modeling regard-

131 ing ash injection height and timing thereof. We use Plume-SPH as an example, noting  
 132 that for other 3D plume models, the steps would be similar. Plume-SPH is a two-phase  
 133 model based on the Lagrangian smoothed-particle hydrodynamics (SPH) method, in which  
 134 the computational domain is discretized by SPH particles. The current version, Plume-  
 135 SPH 1.0 (Cao et al., 2018), uses two types of SPH particles: 1) particles of phase 1 to  
 136 represent ambient air, and 2) particles of phase 2 to represent erupted material. The ini-  
 137 tial ash cloud is created from SPH particles of phase 2.

138 After reaching the maximum rise height and starting to spread horizontally, par-  
 139 ticles of phase 2 form an initial umbrella cloud (Fig. 2). The 3D plume simulation is con-  
 140 sidered complete once the umbrella cloud begins to form. Parcels that will be transported  
 141 by the ambient wind are those above the “corner” region, where mean plume motion is  
 142 horizontal rather than vertical.

143 Considering that SPH particles are only discretization points, each is assigned a  
 144 grain size according to a given total grain size distribution (TGSD) (?), and a concen-  
 145 tration according to the mass and volumetric eruption rate. The Plume-SPH discretiza-  
 146 tion points are thus switched to Puff Lagrangian tracer particles having grain sizes and  
 147 concentrations. The coordinates of these tracer particles, which are initially in the lo-  
 148 cal Cartesian coordinate system of Plume-SPH, are converted into Puff’s global coor-  
 149 dinate system, which is given in terms of (*longitude, latitude, height*). Puff takes the ini-  
 150 tial ash cloud, consisting of the collection of Lagrangian tracer particles with grain size  
 151 and concentration, and propagates from time  $t$  to time  $t+\Delta t$  via an advection/diffusion  
 152 equation (Searcy et al., 1998).

$$153 \mathbf{R}_i(t + \Delta t) = \mathbf{R}_i(t) + \mathbf{W}(t)\Delta t + \mathbf{Z}(t)\Delta t + \mathbf{S}_i(t)\Delta t \quad (1)$$

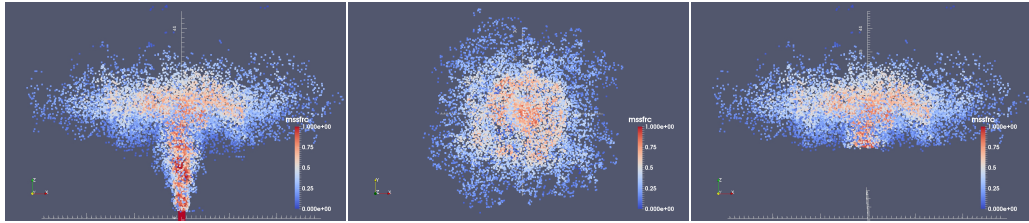
154 Here,  $\mathbf{R}_i(t)$  is the position vector of the  $i^{th}$  Lagrangian tracer particle at time  $t$ ,  $\mathbf{W}$  ac-  
 155 counts for wind advection,  $\mathbf{Z}$  accounts for turbulent dispersion and  $\mathbf{S}$  is the terminal grav-  
 156 itational fallout velocity, which depends on tracer’s size.

157 To summarize, there are four steps to create an initial ash cloud from the raw out-  
 158 put of Plume-SPH:

- 159 1. filter by SPH particle type to select SPH particles that represent erupted mate-  
 160 rial (phase 2)
- 161 2. filter by a mean velocity threshold to select the upper part (above the “corner”  
 162 region) dominated by horizontal transport
- 163 3. switch SPH discretization points to Lagrangian tracer particles, by assigning grain  
 164 size to each particle
- 165 4. convert coordinates of the SPH Lagrangian tracers into the VATDs’ geographic  
 166 coordinate system

167 The features of the volcanic plume and resulting initial ash cloud used in the case study  
 168 are shown in Fig. 2. It is important to point out that since both Plume-SPH and Puff  
 169 are based on the Lagrangian method, there is no extra step of conversion between an Eu-  
 170 lelian grid and Lagrangian particles.

178 Table 1 compares three different methods for creating initial conditions for VATD  
 179 simulation: 1) creating initial condition based on parameter calibration without any plume  
 180 model (method 1), 2) creating initial condition based on output of 1D plume model (method  
 181 2), 3) extracting initial ash cloud from 3D plume simulation (method 3). The first method  
 182 determines all global descriptors of volcanic plumes based on calibration. Then create  
 183 an initial line source or ash cloud according to semiempirical plume shape expression.  
 184 Both other two methods depend on plume models. However 3D plume models can gen-  
 185 erate initial ash clouds in 3D space while 1D plume models only obtain global descrip-  
 186 tors of plume so still need semiempirical expression to create 3D initial ash clouds. In



171 **Figure 2.** All particles in the pictures are of type phase 2 (phase 1 has been removed in step  
 172 1) at 600s after eruption, at which time, the plume has already reached the maximum height  
 173 and started spreading radially. Pictures from left to right are: front view of the whole plume,  
 174 top view of the plume and front view of the initial ash cloud, which is essentially a portion of the  
 175 whole plume with elevation higher than a given threshold (in this picture is 15000m). Particles  
 176 are colored according to mass fraction of erupted material. Red represents high mass fraction  
 177 while blue represents low mass fraction.

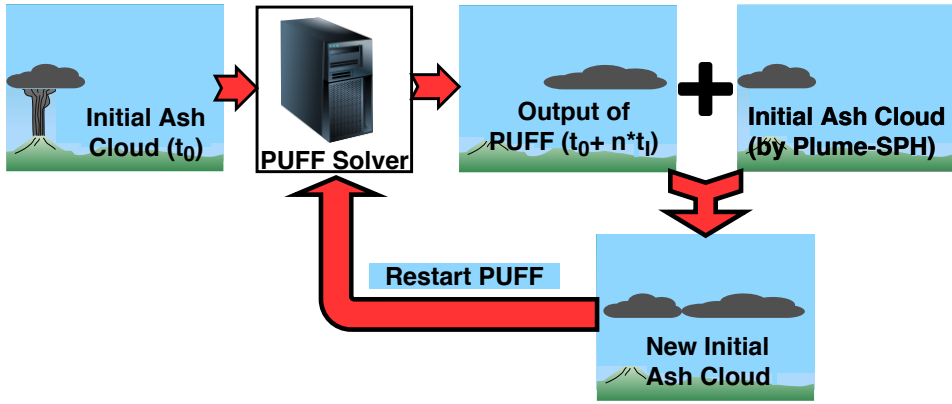
190 **Table 1.** Three different methods for creating initial conditions (initial ash clouds) for Puff  
 191 simulation

	No model	1D model	3D model
Maximum height	Calibration	Semiempirical	1st principle
Average height	Calibration	Conservation laws (1D)	1st principle
Vertical spread	Calibration	Semiempirical	1st principle
Column radius	Calibration	Conservation laws (1D)	1st principle
Plume shape	Semiempirical	Semiempirical	1st principle
Tracers number	Free parameter	Free Parameter	Based on simulation

187 addition, the number of Lagrangian tracers is a free parameter when using semiempirical  
 188 plume shape expressions while it purely depends on simulation when creating ini-  
 189 tial conditions from 3D plume simulation results.

## 192 2.2 Puff Restart

193 The plume and ash transport models are run at different time scales and length  
 194 scales. The spatial and temporal resolutions of the plume simulations are much finer than  
 195 those of the ash transport model. It takes tens of minutes (600s in this case) for the Pinatubo  
 196 plume to reach a steady height. However the eruption persisted for a few hours (9 hours  
 197 for the climactic phase of Pinatubo eruption), and it may be necessary to track ash trans-  
 198 port for days following an eruption. At present, it is too expensive computationally to  
 199 do 3D plume simulations of several hours in real time. In order to handle the difference  
 200 in time scale, we mimic a continuing eruption with intermittent pulsed releasing of ash  
 201 particles. Particularly, we restart Puff at an interval of 600s, i.e., the physical time of  
 202 the plume simulation to reach steady height. At every Puff restart, we integrate the out-  
 203 put of the last Puff simulation and Plume-SPH into a new ash cloud. This new ash cloud  
 204 serves as a new initial condition with which to restart a Puff simulation. The interval  
 205 of the pulsed releases is the simulation time of Plume-SPH, i.e., 600s in our case study.  
 206 A sketch demonstrating the overall restart process is shown in Fig. (3). The total num-  
 207 ber of Lagrangian tracer particles used in Puff thus equals the summed number of par-  
 208 ticles in all releases. So the total number of tracer particles is no longer a user-selected  
 209 parameter. ? proposed using more realistic time-dependent plume heights. We do not  
 210 adopt that strategy here for simplicity, although the idea would be straightforward in  
 211 execution, given time-dependent eruption conditions.



212 **Figure 3.** Mimic successive eruption with intermittent pulsed releasing of ash particles.  $t_I$  is  
213 the period of pulsing release.  $t_I$  equals the physical time of 3D plume simulation.

### 214 2.3 Sensitivity Analysis of Other Parameters

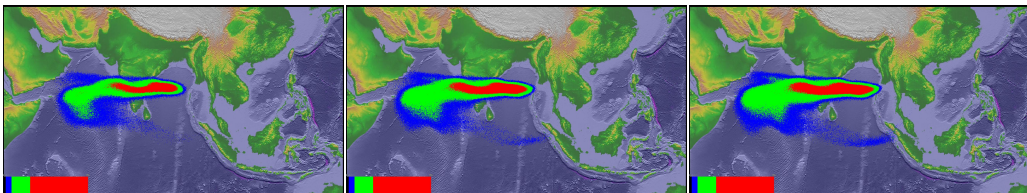
215 Besides the positions of particles in the initial ash cloud, other parameters for Puff  
216 simulations are: horizontal diffusivity, vertical diffusivity, mean grain size, grain size stan-  
217 dard deviation and total number of tracers. We present in this subsection systematic sen-  
218 sitivity studies on these parameters. We also investigate the influence of eruption du-  
219 ration. The sensitivity analyses will serve as the basis for identifying possible sources of  
220 disparities between simulation and observation.

221 The sensitivity analyses illustrate that adjustment of other parameters produces  
222 negligible visual differences in VATD simulation results. Using different vertical diffu-  
223 sivities in range of  $[100, 100000] m^2 s^{-1}$  and different horizontal diffusivities in range of  
224  $[1, 20] m^2 s^{-1}$  produces visually negligible differences. The simulation eruption duration  
225 should depend on the total observed duration or the duration of the climactic phase. We  
226 conducted several simulations with eruption duration varying in range of  $[5, 11] hours$  with  
227 slightly different starting time of climactic phase. Table 2 lists all these simulations. How-  
228 ever, only tiny visible differences are observed among the simulated ash transportation.  
229 The mean of grain size also has visually ignorable effects on long-term ash transporta-  
230 tion according to our sensitivity tests varying the log mean (base 10) grain radius in a  
231 range of  $[-7.3, -3.5] m$ . The standard deviation, when varying in range of  $[0.1, 10]$ , gen-  
232 erates an ignorable difference on long-term ash transportation as well. Similar conclu-  
233 sion on parameter sensitivity is reported by ?Daniele et al. (e.g. 2009). Among these pa-  
234 rameters, the eruption duration and beginning time shows, even though tiny, the most  
235 obvious influence on simulated ash distribution. In order to show such differences in an  
236 intuitive way, Fig. 4 shows simulated ash distribution corresponding to 4.9 hours dura-  
237 tion, 9 hours duration and 11 hours duration respectively. After 72 hours, relative to the  
238 simulation starting time, these three cases generate generally similar results, with high  
239 concentration ash covering almost the same region. The difference of lower concentra-  
240 tion distribution is relatively more obvious. Ash cloud covers the broadest area when the  
241 eruption duration is 11.1 hours. To summarize, all these parameters have either tiny or  
242 ignorable effects on long-term ash distribution simulation.

243 The new methodology for generating initial ash clouds introduces another new pa-  
244 rameter: elevation threshold. We also carry out sensitivity analysis on this parameter  
245 by varying the elevation threshold from  $1500 m$  (the height of the vent) to  $25000 m$ . The  
246 simulated ash distributions show obviously visible differences. Such influence is especially  
247 obvious when the elevation threshold is either very large or very small. However, vary-  
248 ing the elevation threshold in the range of  $[12000, 18000] m$  generates relatively small dif-

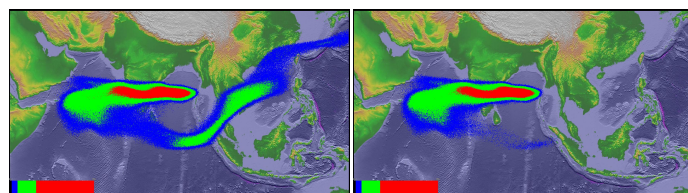
243 **Table 2.** The starting and ending time (UT) for simulating the climactic phase of Pinatubo  
 244 eruption on June 15 1991. Observed plume height (?) at different time are also listed in the  
 245 table.

Eruption duration	4.9 hours	9 hours	10 hours	11.1 hours
Start time	0441	0441	0441	0334
Height at start time	37.5 km	37.5 km	37.5 km	24.5 km
End time	0934	1341	1441	1441
Height at end time	35 km	26.5 km	22.5	22.5 km



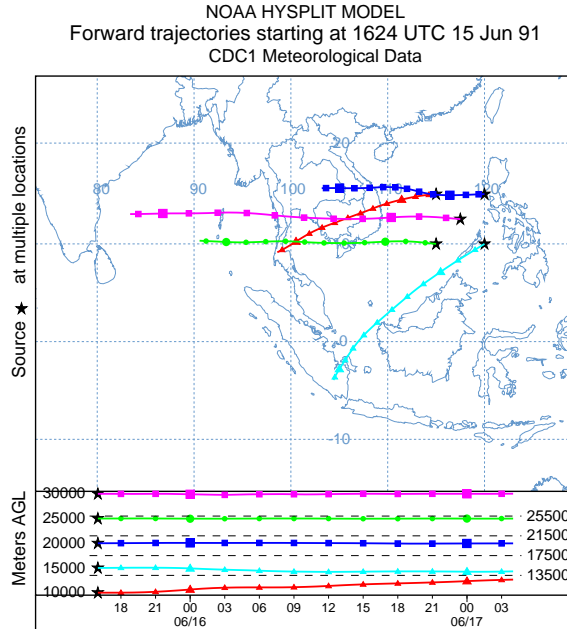
246 **Figure 4.** Simulated ash cloud distribution corresponding to eruption duration of 4.9 hours, 9  
 247 hours and 11.1 hours (from left to right) respectively. Starting and ending time for each case is in  
 248 Table 1. The contours are for ash distribution at 72 hours after eruption.

249 differences in ash transportation simulation results. Figure 5 compares the simulated ash  
 250 distribution corresponding to elevation thresholds of 1500m and 15000m. Compared with  
 251 ash distribution for threshold of 15000m, an extra long tail appears when using eleva-  
 252 tion threshold of 1500m. Adopting smaller elevation thresholds essentially adds more trac-  
 253 ers at lower elevation. As the wind at different elevations are different, these tracers at  
 254 lower elevation would transpose to different directions. The hysplit (??) forward trajec-  
 255 tories tracking, which starting at June 15 1624 UTC, indicates that the wind between  
 256 evaluation 10000 m to 15000 m blows from north-east to south-west while wind of higher  
 257 evaluation blows from east to west (see Fig. 6).



258 **Figure 5.** Simulated ash distribution taking initial ash clouds obtained using different eleva-  
 259 tion thresholds (1500m and 15000 m) from output of Plume-SPH. The contours correspond to  
 260 ash concentration at 72 hours after eruption. The starting and ending time are corresponding to  
 261 9 hours duration case in Table 2

262 The sensitivity analyses demonstrate that the initial condition for VATD simula-  
 263 tion has the most significant effect on simulated ash distribution while all other input  
 264 parameters have either tiny or ignorable influence. The initial ash cloud generated based  
 265 on semiempirical expression, which is a function of several parameters, might be signif-  
 266 icantly disparate from a realistic ash cloud. Such initial conditions might greatly com-  
 267 promise the accuracy of VATDs simulation.



268 **Figure 6.** Trajectories of particles starting from different heights indicating the wind direc-  
269 tions of different evaluations.

276 In this paper, we do not carry out any investigation with respect to wind field even  
277 though it is another dominant factor in VATD simulation. In the case study, we use global  
278 NOAA/OAR/ESRL6 –  $h$ ,  $2.0^\circ$  reanalysis wind fields data (???).

### 279 3 Comparison and Discussion

280 Transportation of volcanic ash resulting from the Pinatubo eruption on June 15th  
281 1991 is simulated using two different initial conditions. The first type of initial condi-  
282 tion is created in a traditional way according to key global descriptors and semiempir-  
283 ical plume shape expression. The second type of initial condition is created by the new  
284 method proposed in this paper. Simulated ash transportation results are compared against  
285 observations.

287 To create initial conditions using the new method described in this paper, the plume  
288 rise is simulated first by Plume-SPH. The eruption parameters, material properties and  
289 atmosphere for the strong plume no wind case in a comparison study on eruptive col-  
290 umn models (Costa et al., 2016) are adopted. Eruption conditions and material prop-  
291 erties are listed in Table 3. Note that the density of erupted material at the vent and

286

**Table 3.** List of eruption condition and material properties for plume simulation

Parameters	Units	Plume
Vent velocity	$m \cdot s^{-1}$	275
Vent gas mass fraction		0.05
Vent Temperature	$K$	1053
Vent height	$m$	1500
Mass discharge rate	$kg \cdot s^{-1}$	$1.5 \times 10^9$
Specific heat of gas at constant volume	$J \cdot kg^{-1} \cdot K^{-1}$	717
Specific heat of air at constant volume	$J \cdot kg^{-1} \cdot K^{-1}$	1340
Specific heat of solid	$J \cdot kg^{-1} \cdot K^{-1}$	1100
Specific heat of gas at constant pressure	$J \cdot kg^{-1} \cdot K^{-1}$	1000
Specific heat of air at constant pressure	$J \cdot kg^{-1} \cdot K^{-1}$	1810
Density of air at vent height	$kg \cdot m^{-3}$	1.104
Pressure at vent height	$Pa$	84363.4

292  
293  
294  
295  
296  
297  
298

radius of the vent can be computed from the given parameters. The eruption pressure is assumed to be the same as the pressure of ambient at the vent and hence is not given in the table. The vertical profiles of atmospheric properties were obtained based on the reanalysis data from ECMWF (European Centre for Medium-Range Weather Forecasts) for the period corresponding to the climactic phase of the Pinatubo eruption. The initial ash cloud is obtained by processing the raw output of Plume-SPH following steps described in Sec. 2.

303  
304  
305  
306  
307  
308  
309

Another set of initial conditions is created based on observed top height (40km) and several other parameters assigned semiempirically (?). These parameters, namely, the global descriptors of volcanic plume, are used as parameters of semiempirical expression to get ash clouds in 3D space. See details in Table 4. Except for initial conditions, the simulation parameters that control VATD simulation are the same for both simulations. As has been shown in the sensitivity analyses section, these parameters have less influence on simulation results than initial condition.

310

### 3.1 “Plume-SPH + Puff” and “Semiempirical Initial Cloud + Puff”

311  
312

The simulation results using different initial conditions are compared with TOMS images and AVHRR BTD ash cloud map in Fig. 7.

322  
323  
324  
325  
326  
327  
328  
329  
330  
331  
332  
333  
334  
335  
336  
337

The differences between simulated ash transportation by “Semiempirical initial cloud +Puff” and “Plume-SPH+Puff” are obvious. The simulated ash concentration based on initial condition created from Plume-SPH is much closer to observation than that based on semiempirical plume shape expression. Around 23 hours and 31 hours after the beginning of the climactic phase, “Plume-SPH + Puff” simulation generates ash images that are generally close to observational images, especially the location where high concentration ash presents. However, these ash at near west to Pinatubo mountain observed in satellite images does not show up in “Plume-SPH + Puff” simulation results. This disparity is very possible due to the fact that the Mountain Pinatubo continued erupting after the climactic phase while our simulation only simulates the climactic phase. The ash released after the climactic phase is not accounted for in our simulation results. The “Semiempirical initial cloud + Puff” simulation, however, forecasts an ash distribution faster and narrower than observation. The location, where the high concentration ash presents, is located to the far northwest of observed ash. Around 55 hours after the beginning of the climactic phase, the disparity between observation and simulation becomes more obvious. Ash distribution of “Semiempirical initial cloud + Puff” simulation lo-

299    **Table 4.** Parameters used in VATD simulation of the climactic phase of Pinatubo eruption on  
 300    June 15 1991. The first six parameters are used by semiempirical expression to create an initial  
 301    ash cloud. When creating an initial condition based on the Plume-SPH model, these parameters  
 302    are extracted from output of Plume-SPH model.

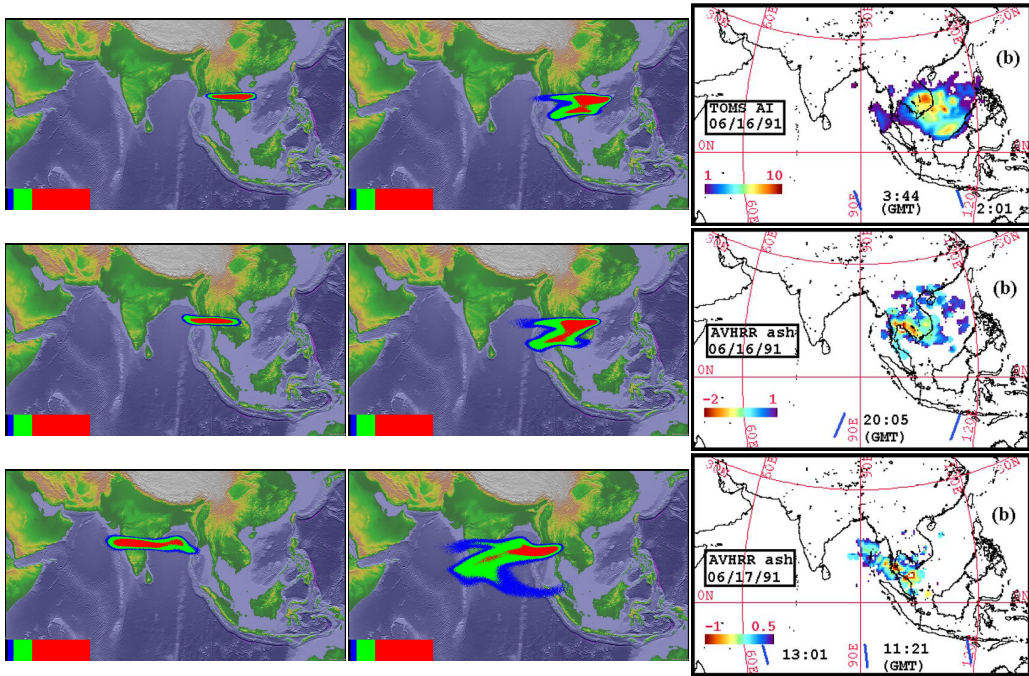
Parameters	Unit	Semiempirical	Plume-SPH
Maximum Height ( $H_{max}$ )	m	40000	41800
Horizontal Spread ( $R_{max}$ )	km	103.808	-
Vertical Spread ( $H_{width}$ )	km	6.662	-
Plume Shape	-	Poisson	-
Total Ash Particles	-	1768500	1768500
Elevation Threshold	m	-	15000
Horizontal Diffusivity	$m^2/s$	10000	10000
Vertical Diffusivity	$m^2/s$	10	10
Grain Size Distribution	-	Gaussian	Gaussian
Mean of Grain Size (Radius)	mm	$3.5 \times 10^{-2}$	$3.5 \times 10^{-2}$
Standard Deviation of Grain Size	-	1.0	1.0
Start Time	UT	0441	0441
End time	UT	1341	1341
Simulation Duration	hour	72	72

338    cates far west to the observed ash. The high concentration area of “Plume-SPH + Puff”  
 339    simulation, even though closer to observation than that of “Semiempirical initial cloud  
 340    +Puff”, is still faster than observation.

341    Except for the initial condition, both simulations adopt the same parameters and  
 342    wind field data. That is to say, the only difference between these two simulations is the  
 343    initial condition. Recall that the initial condition has the most significant influence on  
 344    ash transportation simulation. It is therefore very likely that the big difference between  
 345    simulation results by “Plume-SPH+Puff” and “Semiempirical initial cloud +Puff” may  
 346    be attributed to the initial condition and thereby be credited with its added skill.

### 347    3.2 Discussion Regarding Maximum Height ( $H_{max}$ )

348    In this section, we mainly discuss the vertical distribution of ash particles in the  
 349    initial ash cloud. The majority of volcanic ash particles usually present a lower eleva-  
 350    tion than maximum height. For instance, ?? reported the maximum Pinatubo plume  
 351    height as high as around 39km while the cloud heights were estimated at 20 ~ 25km,  
 352    ? report the maximum plume height could be > 35km and the plume heights are 23 ~  
 353    28km after 15 ~ 16 hours. The neutral buoyant regions of the Pinatubo aerosol esti-  
 354    mated by different measurements are: 17 ~ 26km (lidar) by ?, 20 ~ 23km (balloon)  
 355    by ?, 17 ~ 28km (lidar) by Jäger (1992), and 17 ~ 25km (lidar) by Avdyushin et al.  
 356    (1993). Based on comparison between simulated clouds with early infrared satellite im-  
 357    ages of Pinatubo, ? reported that the majority of ash was transported between 16km  
 358    and 18km. This is physically understandable as particles are concentrated along the in-  
 359    trusion height of the umbrella cloud, not near the top because the plume top is due to  
 360    momentum overshoot. However, the empirical expressions for the height-MER relation,  
 361    which are commonly adopted to create initial conditions for VATD simulation, tend to  
 362    place the majority of ash particles closer to top if use observed maximum height in the  
 363    empirical expressions.



313 **Figure 7.** Comparison between “Semiempirical initial cloud + Puff” and “Plume-SPH +  
 314 Puff”. Pictures from left to right are: Puff simulation based on initial condition created according  
 315 to semiempirical plume shape expression, Puff simulation based on initial condition generated by  
 316 Plume-SPH, TOMS or AVHRR image of Pinatubo ash cloud. Ash clouds at different hours after  
 317 eruption are on different rows. From top to bottom, the images are corresponding to around 23  
 318 hours after eruption (UT 199106160341), 31 hours after eruption (UT 199106161141), 55 hours  
 319 after eruption (UT 199106171141). The observation data on the first row are TOMS ash and ice  
 320 map. The observation data on the second and third row are AVHRR BTD ash cloud map with  
 321 atmospheric correction method applied (?).

364 Here we check two commonly used plume shapes, the Poisson and Suzuki. For Pois-  
 365 son plume shape, the vertical height of ash particles are determined according to Eq. (2).

$$H = H_{max} - 0.5H_{width} * P + H_{width}R \quad (2)$$

366 where  $P$  is an integral value drawn from a Poisson distribution of unit mean,  $R$  is a uni-  
 367 formly distributed random number between 0 and 1,  $H_{max}$  is the maximum plume height,  
 368  $H_{width}$  represents an approximate vertical range over which the ash will be distributed.  
 369 For Suzuki plume shape (T. Suzuki et al., 1983), volcano ash mass vertical distribution  
 370 is assumed to follow the Suzuki equation (Eq. (3)).

$$Q(z) = Q_m * \frac{k^2(1 - z/H_{max})\exp(k(z/H_{max} - 1))}{H_{max}[1 - (1 + k)\exp(-k)]} \quad (3)$$

371 Where  $Q_m$  is the total mass of erupted material,  $k$  is shape factor, which is an adjust-  
 372 able constant that controls ash distribution with height. A low value of  $k$  gives a roughly uni-  
 373 form distribution of mass with elevation, while high values of  $k$  concentrate mass near  
 374 the plume top.

375 Particle distribution (in terms of mass percentage or particle number percentage)  
 376 in vertical direction in the initial ash cloud are shown in Fig. 8. In that figure, the ver-  
 377 tical particle distribution based on Plume-SPH output is compared with vertical par-  
 378 ticle distribution created based on semiempirical shape expressions. Both Poisson and

Suzuki distribution in Fig. 8 take  $H_{max} = 40000m$ , which is close to reported observation of maximum height. When adopting Poisson plume shape, the majority of the particles are between  $30km \sim 40km$ . Obviously, Poisson distributes majority ash at a much higher elevation than observations (e.g. ?). As for Suzuki, the majority of ash particles also distribute in a range that is significantly higher than  $25km$ . As for initial ash clouds based on Plume-SPH simulation, the major population of ash particles distribute between  $17km \sim 28km$ , which match well with observations. The maximum height is also consistent with observation. To summarize, using semiempirical plume shape expression generates an unrealistic initial ash cloud even if we use observed plume maximum height.

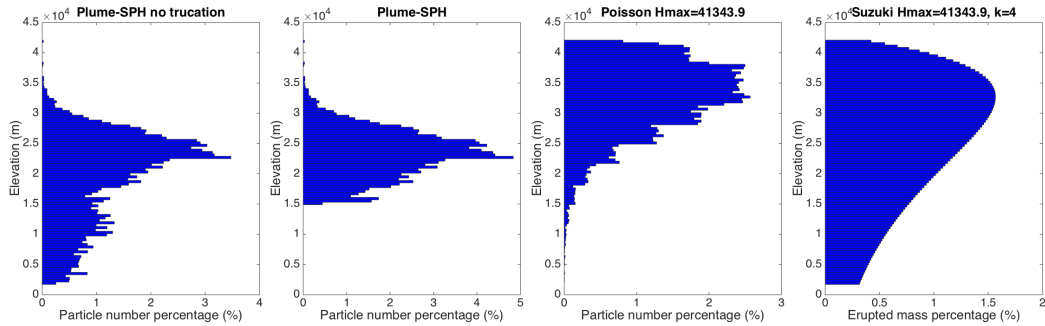
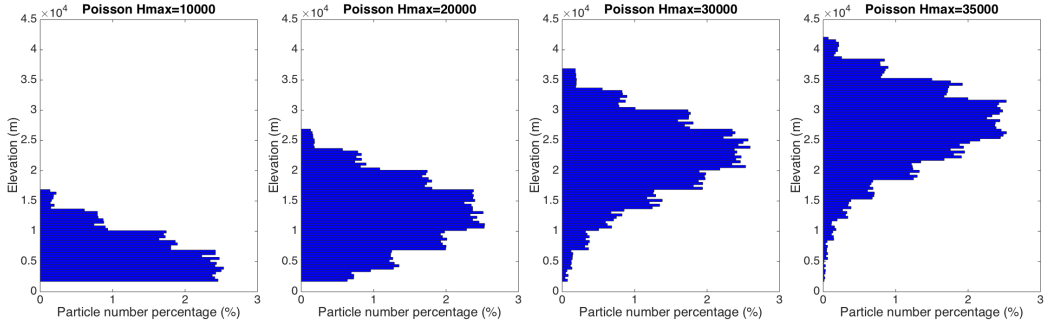


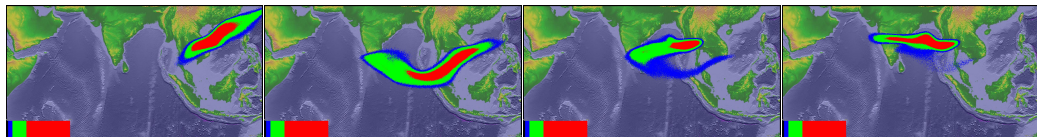
**Figure 8.** Particle distribution of initial ash cloud in vertical direction. The picture to the left is corresponding to the initial ash cloud obtained from Plume-SPH output. The second picture is corresponding to ash distribution truncated by a elevation threshold of  $15000m$ . The third picture is for vertical ash distribution based on Poisson distribution with maximum height equals to  $40000m$ . Another parameter, the vertical spread, in the expression of Poisson plume shape is  $6662m$ . The picture to the right is corresponding to Suzuki distribution with maximum height equals to  $40000m$ . Another parameter in Suzuki distribution, the shape factor, is 4. The  $x$  axis is the percentage of particle numbers for Plume-SPH and Poisson. For Suzuki the  $x$  axis is the mass percentage of erupted material.

For Poisson and Suzuki plume shape, vertical distribution of ash particles can't be lower down without changing the maximum height. To distribute a major population of ash particles at lower elevation, the maximum height has to be reduced to a value smaller than observed maximum height. Adjusting parameters such as maximum height in the empirical expression is actually the traditional source term calibration method. A set of initial ash clouds using different maximum heights based on Poisson plume shape is shown in Fig. 9). The maximum heights adopted in plume shape expressions are, by no means, obtained from any plume model or observation. Except for maximum height, all other parameters for creating an initial ash cloud are the same as these in Table 4. The range, between which major populations of ash particles locate, is lower when using smaller maximum heights. These ash clouds created by Poisson distribution with different maximum heights are then used as initial conditions in Puff simulation, whose results are shown in Fig. 10.

Figure 10 shows that the maximum height has significant influence on ash transportation simulation. When the maximum height is  $10000m$  the high concentration area is lag behind observation. While the designated maximum height is  $35000m$ , the high concentration area is a little bit faster and much narrower than observation. When using a maximum height of  $41343.9m$ , the high concentration area is faster and narrower than both observation and “Pume-SPH+Puff” simulation results (see Fig. 7). The simulated high concentration area is closest to “Pume-SPH+Puff” simulation results when



411 **Figure 9.** Initial particle distribution in vertical direction based on Poisson plume shape with  
 412 different maximum heights. Pictures from left to right are corresponding to maximum height of  
 413 10000m, 20000m, 30000m, 35000m. Another parameter, the vertical spread, in the expression of  
 414 Poisson plume shape is 6662m for all cases. The  $x$  axis is the percentage of particle numbers. See  
 415 Fig. 8 for vertical ash distribution of Plume-SPH output.



416 **Figure 10.** Ash transportation simulated by Puff using different initial ash clouds created  
 417 according to Poisson distribution with different maximum heights. Pictures from left to right are  
 418 corresponding to maximum plume heights of 10000m, 20000m, 30000m and 35000m. All images  
 419 are for simulated ash transportation around 55 hours after eruption (UT 199106171141). See the  
 420 observed cloud image in Fig. 7.

428 assigning a maximum height of 30000m. The front of volcano ash, with lower concen-  
 429 tration is faster than observation located far west to high concentration areas. A lower  
 430 concentration tailing area also appears in the simulation results while there is no such  
 431 tail in the observed image. Puff simulation result based on calibrated maximum height  
 432 of 30000m shows similar footprint to, even though smaller in terms of covered area than,  
 433 those of "Pume-SPH+Puff" simulation. However, the initial ash cloud created by Pois-  
 434 son distribution with maximum height around 20000m generates best match ash distri-  
 435 bution with observation. That is to say, a maximum height lower than real maximum  
 436 height is required by Poisson plume shape to distribute ash particles at the same eleva-  
 437 tion as real ash distribution. This is physically understandable as maximum plume heights  
 438 are reached due to overshoot. Our hypothesis regarding the sources of disparity between  
 439 "Semiempirical initial cloud +Puff" simulation and observation is confirmed. Since the  
 440 initial condition has such a dominant effect on VATD simulation, it is critical for the fore-  
 441 cast capability of VATD simulation to explore the more accurate and adaptive ways for  
 442 establishing the initial conditions, especially the method that does not rely on "post event"  
 443 parameter calibration.

### 444 3.3 Discussion Regarding Vertical Spread ( $H_{width}$ )

445 In the previous section, the maximum height is adjusted to change vertical ash dis-  
 446 tribution along the source line. This section investigates another parameter in semi em-  
 447 pirical Poisson expression. We vary the "vertical spread" ( $H_{width}$ ) in range 3km/ 10km.  
 448 A set of initial ash clouds created according to different "vertical spread" is shown in Fig.  
 449 11. Except for "vertical spread", all other parameters for creating an initial ash cloud  
 450 are the same as these in Table 4. Width of the range within which major populations

of ash particles locate become narrower when a smaller value for vertical spread is used. But changing  $H_{width}$  has no obvious effect on the height at which the majority of ash particles distribute. These ash clouds based on different vertical spread are then used as initial conditions in Puff simulation, whose results are shown in Fig. 12.

Adjusting of the vertical spread can change particle distribution in vertical direction and not surprisingly affect VATD simulation results. Unluckily, none of these VATD simulations based on initial ash cloud with vertical spread equals to 3km, 5km, and 10km get better results than VATD simulation based on initial condition created by a 3D plume simulation using Plume-SPH (see Fig. 12).

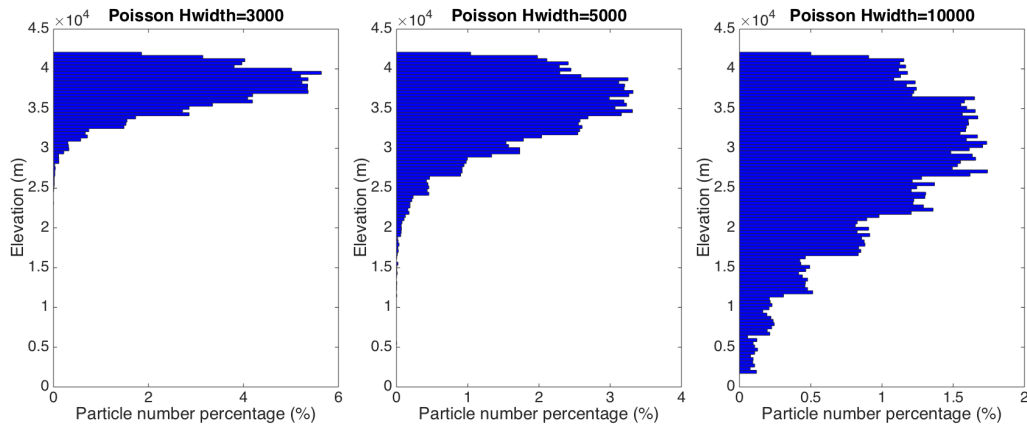


**Figure 11.** Vertical particle distribution based on Poisson plume shape with different “vertical spread”. Pictures from left to right are corresponding to vertical spread of 3km, 5km and 10km. The maximum height in the expression of Poisson plume shape is 40000m for all cases. The  $x$  axis is the percentage of particle numbers. See Fig. 8 for vertical ash distribution of Plume-SPH output.

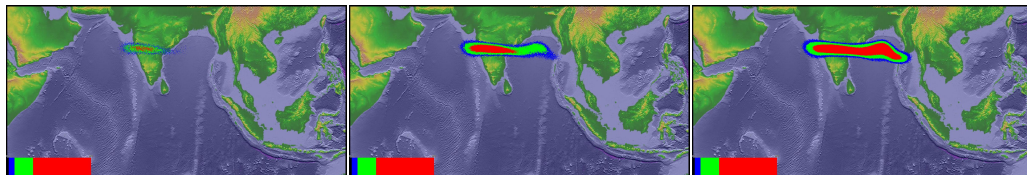


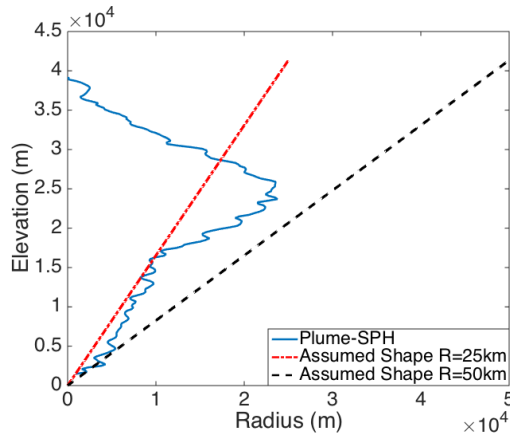
**Figure 12.** Ash transportation simulated by Puff using different initial ash clouds created with different vertical spread. Pictures from left to right are: Puff simulation results based on initial ash clouds with vertical spread equals to 3000mm, 5000mm and 10000m. The images are corresponding to around 55 hours after eruption (UT 199106171141). See the observed cloud image in Fig. 7. The simulated ash field does not adequately cover the observed ash field.

The calibrations carried out here are definitely not exhaustive. One might do more comprehensive calibration throughout the multi-dimensional parameter space (for Poisson distribution, the parameter space is two dimensional) and get better matched ash transportation results. With more complicated plume shape expression, one could have more control over plume shape and might be able to get an initial condition that is much closer to the actual initial ash cloud, hence obtaining more accurate ash transportation prediction. But more complicated plume shape expression usually leads to higher dimensional parameter space which requires more effort to do calibration. Even though, the

478 degree of freedom to adjust plume shape is still limited. The new method for creating  
 479 initial conditions based on 3D plume simulation is more adaptive to various cases and  
 480 obviates semi empirical expressions regarding plume shape.

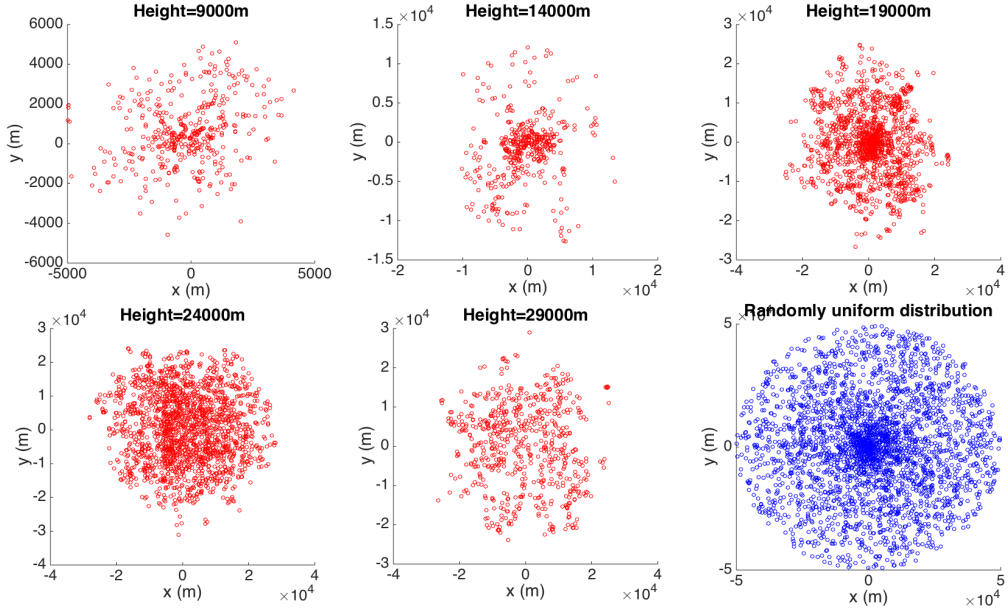
### 481 3.4 Horizontal Ash Distribution

482 The differences between assumed plume particle distribution and actual (or sim-  
 483 ulated by 3D plume) model are not only in vertical direction. Dependence on hori-  
 484 zontal particle distribution of the initial ash cloud on ash transportation is investigated in  
 485 this section. Puff uses a uniformly distributed random process to determine the ash par-  
 486 ticle location in a circle centered on the volcano site. The maximum radius (at top) is  
 487 given as “horizontal spread” in Table 4. The horizontal displacement from a vertical line  
 488 above the volcano is a random value within a circle of radius, which equals to “horiz-  
 489 onal spread” multiplied by the ratio of the particle height  $H$  to maximum  $H_{max}$ . So the  
 490 net shape of the plume is an inverted cone where particles are located directly over the  
 491 volcano at the lowest level and extend out further horizontally with increasing plume height.  
 492 As for output of Plume-SPH, an effective radius is determined according to a given thresh-  
 493 old of ash concentration following Cerminara, Esposti Ongaro, & Neri (2016). A time  
 494 averaging and spatial integration of the dynamic 3D flow fields are conducted to get rid  
 495 of significant fluctuations in time and space. Fig. 13 compares radius of initial ash clouds  
 496 created by 3D plume simulation and assumed plume shape expression adopted in Puff.  
 497 Obviously, It is impossible for the simple assumed plum shapes to capture the complex  
 498 and more realistic shapes developed by 3D plume simulation of Plume-SPH. Additional  
 499 parameterization may generate more reasonable shapes but none are likely to have the  
 500 fidelity of the 3D simulation.



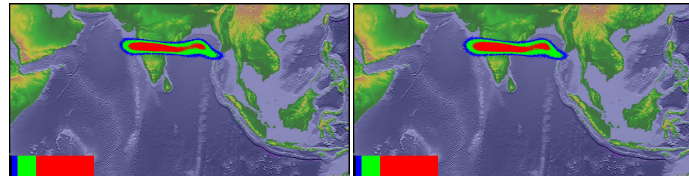
501 **Figure 13.** Comparison between radius of initial ash clouds created by 3D plume model  
 502 (Plume-SPH) and assumed initial ash cloud shape in Puff. The plume shape expression used in  
 503 Puff defines an inverted cone whose actual shape changes when “horizontal spread” takes differ-  
 504 ent values.  $R = 25\text{km}$  is corresponding to “horizontal spread” equals to  $50\text{km}$ .  $R = 50\text{km}$  is  
 505 corresponding to “horizontal spread” equals to  $100\text{km}$

506 Comparison between cross-sectional views of the initial ash clouds is shown in Fig.  
 507 14. The cross-sectional view of assumed plume shape (last figure in Fig. 14) is similar  
 508 to a cross-sectional view of simulated 3D plumes in general sense. However, for simu-  
 509 lated 3D plume, the ash particle distribution on cross section varies along with height.  
 510 It is hard for semiempirical expressions to have such a distribution. In Puff, particle dis-  
 511 tribution on cross sections is assumed to be the same.



512 **Figure 14.** Horizontal distribution of ash particles (tracers) on a cross section of initial ash  
 513 clouds. Puff assumes a randomly uniform distribution of ash particles within a circle, as shown  
 514 by blue dots in the last figure. All other figures show the ash particle distribution of initial ash  
 515 clouds created by Plume-SPH at different elevations.

516 Assigning different values to “horizontal spread” has an ignorable effect on VATD  
 517 simulation results. We use numbers between  $50\text{km}$  to  $1600\text{km}$  as “horizontal spread” to  
 518 create initial ash clouds for VATD, all of them generate very similar results. Figure 15  
 519 shows two different simulation results based on initial ash clouds with “horizontal spread”  
 520 equals to  $50\text{km}$  and  $600\text{km}$  respectively. No visible differences are apparent between them.  
 521 This implies that horizontal distribution has less significant influence on VATD simu-  
 522 lation results than vertical distribution.



523 **Figure 15.** Ash transportation simulated by Puff at around 55 hours after eruption (UT  
 524 199106171141). Different values for “horizontal spread” are used to create an initial ash cloud.  
 525 Pictures to the left are corresponding to “horizontal spread” equals to  $50\text{kmm}$ . Pictures to the  
 526 right corresponding to “horizontal spread” equals to  $600\text{kmm}$ . The observed cloud image is in  
 527 Fig. 7.

## 528 4 Conclusion

529 This paper presented, for the first time, VATD simulations using initial source con-  
 530 ditions created by a 3D plume model. Traditional VATD simulations use initial condi-  
 531 tions created according to a semiempirical plume shape expression. A case study of the

532 1991 Pinatubo eruption demonstrates that a 3D plume model can create more realistic  
 533 initial ash cloud and ash parcel positions, and therefore improve the accuracy of ash trans-  
 534 port forecasts. Informal sensitivity analyses suggest that initial conditions, as expressed  
 535 in the disposition of initial ash parcel positions in the vertical, have a more significant  
 536 effect on a volcanic ash transport forecast than most other parameters. Comparison of  
 537 initial ash parcel distributions among the 3D plume model, semiempirical expressions,  
 538 and observations suggests that a major subpopulation of ash parcels should be placed  
 539 at a much lower elevation than maximum height to obtain a better VATD forecast. For  
 540 the Pinatubo case study, “well-matched” simulation results are observed when using a  
 541 maximum height of around 30km, which is much lower than the observed maximum height  
 542 of 40km. Comparing the effects of the maximum height, vertical spread and horizontal  
 543 spread shows that ash particle distribution in the vertical direction has the strongest ef-  
 544 fect on VATD simulation.

545 To summarize, we have presented a novel method for creating *a priori* initial source  
 546 conditions for VATD simulations. We have shown that it might be possible to obtain ini-  
 547 tial positions of ash parcels with deterministic forward modeling of the volcanic plume,  
 548 obviating the need to attempt to obtain initial positions or a history of release heights  
 549 via inversion (Stohl et al., 2011). Although the method now suffers from the high com-  
 550 putational cost associated with 3D forward modeling, it not only helps overcome short-  
 551 comings of existing methods used to generate *a priori* input parameters, but also over-  
 552 comes the need to do the thousands of runs associated with inverse modeling. In addi-  
 553 tion, computational cost will continue to diminish as computing speed increases. As they  
 554 are forward numerical models based on first principles, 3D plume models need little if  
 555 any parameterization, and user intervention should not be required to improve forecast  
 556 power; no assumption about the initial position of ash parcels is needed. Generation of  
 557 the initial cloud of ash parcels directly by 3D simulation is potentially adaptable to a  
 558 variety of volcanic and atmospheric scenarios. In contrast, semiempirical expressions used  
 559 to determine initial conditions require several parameters to control ash particle distri-  
 560 bution along a vertical line source or some simplified shape of the initial ash cloud, mak-  
 561 ing it difficult in some cases to generate initial conditions that closely resemble a com-  
 562 plex reality.

563 The full range of research issues raised by numerical forecasting of volcanic clouds  
 564 is diverse. We described in this paper the effect of initial conditions chosen from the out-  
 565 put of a 3D plume model on numerical forecasts of volcanic ash transport simulation.  
 566 The wind field, another important factor in volcanic ash transportation simulation is not  
 567 discussed in the present work. Some other aspects, such as small scale physical processes,  
 568 even though they play lesser roles, might need to be included in VATDs to improve ac-  
 569 curacy for a particular eruption. In addition, eruption conditions are subject to change  
 570 with time, even during the climactic phase of an eruption. In the future, time-dependent  
 571 initial conditions for VATDs can be created from 3D plume simulations with time-dependent  
 572 eruption conditions.

### 573 Acknowledgments

574 Support for the Twentieth Century Reanalysis Project dataset is provided by the U.S.  
 575 Department of Energy, Office of Science Innovative and Novel Computational Impact  
 576 on Theory and Experiment (DOE INCITE) program, and Office of Biological and En-  
 577 vironmental Research (BER), and by the National Oceanic and Atmospheric Adminis-  
 578 tration Climate Program Office.

### 579 References

580 (n.d.).

- 581 Avdyushin, S., Tulinov, G., Ivanov, M., Kuzmenko, B., Mezhuev, I., Nardi, B., ...  
 582 Chanin, M.-L. (1993). 1. spatial and temporal evolution of the optical thick-  
 583 ness of the pinatubo aerosol cloud in the northern hemisphere from a network of  
 584 ship-borne and stationary lidars. *Geophysical research letters*, 20(18), 1963–1966.
- 585 Bonadonna, C., & Houghton, B. (2005). Total grain-size distribution and volume of  
 586 tephra-fall deposits. *Bulletin of Volcanology*, 67(5), 441–456.
- 587 Bursik, M. (2001). Effect of wind on the rise height of volcanic plumes. *Geophys.  
 588 Res. Lett.*, 28(18), 3621–3624.
- 589 Cao, Z., Patra, A., Bursik, M., Pitman, E. B., & Jones, M. (2018). Plume-sph 1.0:  
 590 a three-dimensional, dusty-gas volcanic plume model based on smoothed particle  
 591 hydrodynamics. *Geoscientific Model Development*, 11(7), 2691–2715.
- 592 Cerminara, M., Esposti Ongaro, T., & Berselli, L. (2016). Ashee-1.0: a compressible,  
 593 equilibrium-eulerian model for volcanic ash plumes. *Geoscientific Model Develop-  
 594 ment*, 9(2), 697–730.
- 595 Cerminara, M., Esposti Ongaro, T., & Neri, A. (2016). Large eddy simulation of  
 596 gas-particle kinematic decoupling and turbulent entrainment in volcanic plumes.  
 597 *Journal of Volcanology and Geothermal Research*.
- 598 Costa, A., Suzuki, Y., Cerminara, M., Devenish, B., Esposti Ongaro, T., Herzog, M.,  
 599 ... others (2016). Results of the eruptive column model inter-comparison study.  
 600 *Journal of Volcanology and Geothermal Research*.
- 601 Daniele, P., Lirer, L., Petrosino, P., Spinelli, N., & Peterson, R. (2009). Applications  
 602 of the puff model to forecasts of volcanic clouds dispersal from etna and vesuvio.  
 603 *Computers & Geosciences*, 35(5), 1035–1049.
- 604 de'Michieli Vitturi, M., Neri, A., & Barsotti, S. (2015). Plume-mom 1.0: A new  
 605 integral model of volcanic plumes based on the method of moments. *Geoscientific  
 606 Model Development*, 8(8), 2447–2463.
- 607 Draxler, R. R., & Hess, G. (1998). An overview of the hysplit\_4 modelling system for  
 608 trajectories. *Australian meteorological magazine*, 47(4), 295–308.
- 609 D'amours, R. (1998). Modeling the etex plume dispersion with the canadian emer-  
 610 gency response model. *Atmospheric Environment*, 32(24), 4335–4341.
- 611 Folch, A., Costa, A., & Macedonio, G. (2009). Fall3d: A computational model for  
 612 transport and deposition of volcanic ash. *Computers & Geosciences*, 35(6), 1334–  
 613 1342.
- 614 Folch, A., Costa, A., & Macedonio, G. (2016). Fplume-1.0: An integral volcanic  
 615 plume model accounting for ash aggregation. *Geoscientific Model Development*,  
 616 9(1), 431.
- 617 Jäger, H. (1992). The pinatubo eruption cloud observed by lidar at garmisch-  
 618 partenkirchen. *Geophysical research letters*, 19(2), 191–194.
- 619 Mastin, L. G. (2007). A user-friendly one-dimensional model for wet volcanic  
 620 plumes. *Geochemistry, Geophysics, Geosystems*, 8(3).
- 621 Neri, A., Esposti Ongaro, T., Macedonio, G., & Gidaspow, D. (2003). Multiparti-  
 622 cle simulation of collapsing volcanic columns and pyroclastic flow. *Journal of Geo-  
 623 physical Research: Solid Earth (1978–2012)*, 108(B4).
- 624 Oberhuber, J. M., Herzog, M., Graf, H.-F., & Schwanke, K. (1998). Volcanic plume  
 625 simulation on large scales. *Journal of Volcanology and Geothermal Research*,  
 626 87(1), 29–53.
- 627 Pouget, S., Bursik, M., Singla, P., & Singh, T. (2016). Sensitivity analysis of a one-  
 628 dimensional model of a volcanic plume with particle fallout and collapse behavior.  
 629 *Journal of Volcanology and Geothermal Research*.
- 630 Schwaiger, H. F., Denlinger, R. P., & Mastin, L. G. (2012). Ash3d: A finite-volume,  
 631 conservative numerical model for ash transport and tephra deposition. *Journal of  
 632 Geophysical Research: Solid Earth*, 117(B4).
- 633 Searcy, C., Dean, K., & Stringer, W. (1998). Puff: A volcanic ash tracking and pre-  
 634 diction model. *Journal of Volcanology and Geothermal Research*, 80, 1–16.

- 635 Stohl, A., Prata, A., Eckhardt, S., Clarisse, L., Durant, A., Henne, S., ... others  
636 (2011). Determination of time-and height-resolved volcanic ash emissions and  
637 their use for quantitative ash dispersion modeling: the 2010 eyjafjallajökull erup-  
638 tion. *Atmospheric Chemistry and Physics*, *11*, 4333–4351.
- 639 Suzuki, T., et al. (1983). A theoretical model for dispersion of tephra. *Arc volcan-  
640 ism: physics and tectonics*, *95*, 113.
- 641 Suzuki, Y., & Koyaguchi, T. (2009). A three-dimensional numerical simulation of  
642 spreading umbrella clouds. *Journal of Geophysical Research: Solid Earth (1978–  
643 2012)*, *114*(B3).
- 644 Suzuki, Y. J., Koyaguchi, T., Ogawa, M., & Hachisu, I. (2005). A numerical study  
645 of turbulent mixing in eruption clouds using a three-dimensional fluid dynamics  
646 model. *Journal of Geophysical Research: Solid Earth*, *110*(B8).
- 647 Tanaka, H. (1991). Development of a prediction scheme for the volcanic ash fall  
648 from redoubt volcano. In *First int'l. symp. on volcanic ash and aviation safety*  
649 (Vol. 58).
- 650 Tupper, A., Itikarai, I., Richards, M., Prata, F., Carn, S., & Rosenfeld, D. (2007).  
651 Facing the challenges of the international airways volcano watch: the 2004/05  
652 eruptions of manam, papua new guinea. *Weather and Forecasting*, *22*(1), 175–  
653 191.
- 654 Walko, R., Tremback, C., & Bell, M. (1995). Hypact: The hybrid particle and con-  
655 centration transport model. *User's guide*.
- 656 Witham, C., Hort, M., Potts, R., Servranckx, R., Husson, P., & Bonnardot, F.  
657 (2007). Comparison of vaac atmospheric dispersion models using the 1 november  
658 2004 grimsvötn eruption. *Meteorological Applications*, *14*(1), 27–38.
- 659 Woods, A. (1988). The fluid dynamics and thermodynamics of eruption columns.  
660 *Bulletin of Volcanology*, *50*(3), 169–193.
- 661 Zidikheri, M. J., Lucas, C., & Potts, R. J. (2017). Estimation of optimal dispersion  
662 model source parameters using satellite detections of volcanic ash. *Journal of Geo-  
663 physical Research: Atmospheres*, *122*(15), 8207–8232.